Chapter 2

Anomalous Transmission Properties Modulated by Photonic Crystal Bands

Guoyan Dong

Additional information is available at the end of the chapter

http://dx.doi.org/10.5772/intechopen.71403

Abstract

Photonic crystals (PhCs) can be utilized to control the propagation behaviors of light within a frequency band (i.e., conduction band or stop band) for their periodic arrangements of dielectric. Utilizing the effect of band gap one may introduce defects in a photonic crystal to limit or guide the electromagnetic wave with the frequency in stop gaps. Furthermore, based on synthetic periodic dielectric materials photonic crystals can exhibit various anomalous transmission properties, such as negative refraction, self-focusing, zero phase delay or effective-zero-index properties that are determined by the characteristics of their band structures and equal frequency contours (EFC). These extraordinary results contributing to the design of novel PhC devices and the development of PhC application are demonstrated in this chapter.

Keywords: photonic crystal, photonic band gap, negative refraction, zero phase delay, Dirac-like point

1. Introduction

Photonic crystals (PhCs) are structures in which the dielectric constant is periodically modulated on a length scale comparable to the desired wavelength of operation [1, 2], and the resultant photonic dispersion may exhibit photonic band gaps (PBGs) and anomalous propagation behaviors which are useful in controlling light behavior according to different theoretical principles. Based on the PBG effect we may introduce a line defect in a photonic crystal to guide the electromagnetic waves with the frequency in stop gap [3]. The line defect is called a photonic crystal waveguide (PCW), which is very compact (with the typical width is around half-wavelength) and allows sharp bends without losses for its all-dielectric structure [4]. Many attempts have been made to fabricate materials with complete photonic

band gaps (PBGs) at near-infrared [5] and visible frequencies [6], such as semiconductor microfabrication [7], self-assembly of colloidal particles [8], electron-beam lithography [9], multiphoton polymerization [10], holographic lithography (HL) [11], and so on. Among them, HL is a very promising technique for the inexpensive fabrication of high-quality two- and three-dimensional (2D and 3D) PhC templates with the unique advantages of one-step recording, the ability to obtain an inverse lattice by using a template, inexpensive volume recording and rapid prototyping. The PhCs formed by HL which usually have irregular "atoms" or columns. Since the PBG property of resultant structure varies with the shape of "atoms" or columns, thus the PBGs and propagation properties for PhCs made by HL will be different from those of regular structures.

Veselago predicted a kind of materials with negative refractive index in 1968 [12] which has attracted lots of attention in recent years. Such materials are generally referred to as left-handed materials (LHMs), double negative materials [13], or backward-wave media et al. [14], whose best known characteristic is to refract light in opposite direction. Shelby et al. have accomplished one of the first experiments to demonstrate the negative-index behavior [15]. However, the absorption loss of the metal limits its potential optical applications. Different from LHMs, PhCs made of periodic all-dielectric materials can exhibit an fascinating dispersion such as negative refraction and self-focusing properties which are determined by the properties of their band structures and equal frequency contours (EFC) [16, 17].

In this chapter, the maximal complete relative photonic band gaps of 22.1% and 25.1% are introduced how to be achieved in 2D- and 3D photonic crystals formed by HL method. The symmetry mismatch between the incident wave and the Bloch modes of PhC can be used to guide light efficiently. The unique features of negative refraction, dual-negative refraction, triple refraction phenomena, and special collimation effects of symmetrical positive-negative refraction have been verified by numerical simulations or experiments. Effective measurement method has been proposed to identify the Dirac-like point of finite PhC arrays accurately. A mechanism for generation of efficient zero phase delay of electromagnetic wave propagation based on wavefront modulation is investigated with parallel wavefronts (or phasefronts) extending along the direction of energy flow. The band structures of PBG are calculated by the plane-wave expansion method [18], and a finite-difference time-domain (FDTD) method [19] is used to calculate the transmission property of the guided mode. The method of wave-vector diagram is generally used to predict the properties of beam propagation in PhCs.

2. Characteristics of photonic band gap in 2D- and 3D-PhCs

2.1. Photonic band gap in 2D-PhCs

Since the shape and size of lattice columns in 2D case or atoms in 3D case are usually determined by the isointensity surfaces of the interference field, the columns or atoms formed by this way often are of irregular shapes [20, 21]. Consequently, the PBG property of resultant structure is closely related to the fabrication process. Therefore the complete PBG can be obtained and improved by proper designs of the shape and size of lattice cells [22]. Compared with the 3D

case, the 2D PhCs are easier to fabricate and study theoretically for the fact that, the wave propagation of 2D PhCs can be investigated separately for two orthogonal polarizations known as TM and TE. They have important practical significance because they offer the possibility of guiding and manipulating light in planar defect circuits [23], photonic crystal fibers [24] and controlling polarization through their anisotropic band structures.

A kind of 2D 3-fold PhCs conforming to the hybrid triangular configuration formed by HL was proposed [20]. This kind of hybrid triangular lattice is formed by two sets of triangular lattices, as depicted in **Figure 1**, with the big dots indicating the triangular lattice sites with lattice constant a, while the small dots with the same lattice structure shifting $\sqrt{3}a/3$ in y direction. Different from the 6-fold rotational symmetry of regular triangular lattice structure, this hybrid structure has 3-fold rotational symmetry.

The basis vectors of the hybrid triangular lattice may be chosen as $\boldsymbol{a}_1 = a(1/2, \sqrt{3}/2)$ and $\boldsymbol{a}_2 = a(-1, 0)$. To produce this 2D hybrid triangular lattice holographically, we may use the following intensity of interference field,

$$I = 3 + \cos\left[\frac{2\pi}{a}\left(x - \frac{y}{\sqrt{3}}\right)\right] + \cos\left[\frac{2\pi}{a}\left(x + \frac{y}{\sqrt{3}}\right)\right] + \cos\left(\frac{4\pi}{\sqrt{3}a}y\right)$$
$$+c\left\{\cos\left[\frac{2\pi}{a}\left(x - \left(\frac{y}{\sqrt{3}} - \frac{1}{3}\right)\right)\right] + \cos\left[\frac{2\pi}{a}\left(x + \left(\frac{y}{\sqrt{3}} - \frac{1}{3}\right)\right)\right] + \cos\left(\frac{4\pi}{\sqrt{3}a}\left(y - \frac{\sqrt{3}}{3}\right)\right)\right\}, \tag{1}$$

where the first constant has no essential effect, which can be changed by adjusting the light intensity threshold I_t. The former and latter three cosine terms in this formula define the above mentioned two sets of triangular lattices, respectively. The constant c is a modulation coefficient which has a considerable effect on the final structure and thus the corresponding PBGs.

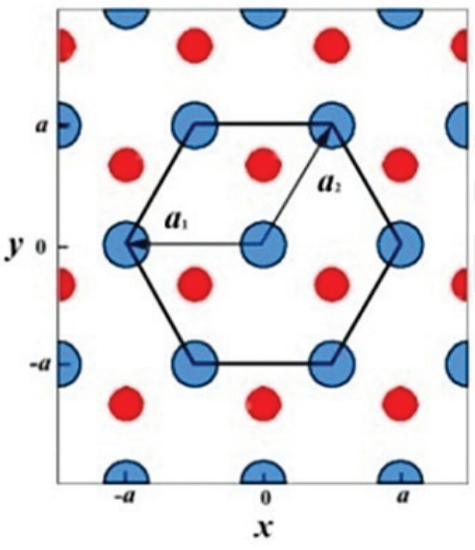

Figure 1. Hybrid triangular lattice with the big dots define a triangular lattice while the small dots compose a same one with a shift of $\sqrt{3}a/3$ in y direction.

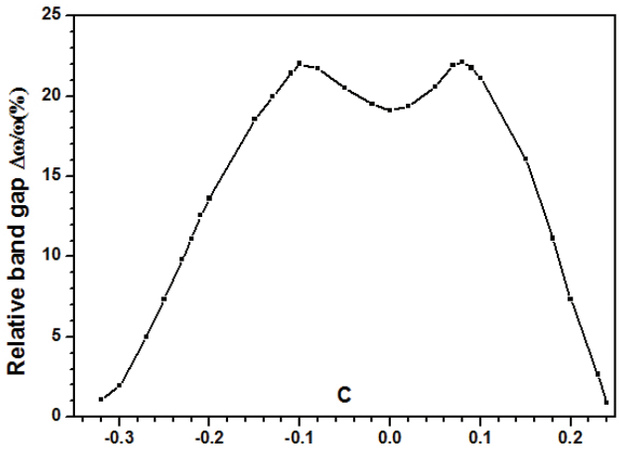

Figure 2. Relation between the value of c and the corresponding maximum relative band width when $\varepsilon = 13.6$. The two peaks of relative band gap occur at $c = -0.1$ and 0.08.

It is clear that the factors of c and I_t can be modulated to control the PBGs. For a given c, a certain lattice structure can be formed by washing away the region of $I < I_t$. If we fill this structure with a material of high refractive index, such as GaAs, and then remove the template, an inverse structure can be achieved as has been successfully demonstrated in Ref. [25]. **Figure 2** represents the relative gap size of optimized structures as a function of c for the dielectric constant contrast of 13.6 to 1 corresponding to GaAs in air. Obviously, the band gaps of PhCs made by HL may be widened from 18.9 to 22.1% by introducing irregularity of the columns and lowering the symmetry of the structure.

In addition, another kind of 2D 6-fold hybrid triangular configuration formed holographically is proposed [21], in which the complete PBGs can be found even with much lower dielectric constant ($\varepsilon = 3.8$). This 2D periodic structure is a hybrid triangular lattice combining two sets of triangular sublattices as depicted in **Figure 3**, where the red dots denote a triangular sublattice with lattice constant a, while the blue dots denote another set with the lattice constant of $a/\sqrt{3}$ which is rotated by an angle of 30° with respect to the former.

For the triangular structure formed holographically the complete PBGs always appear in inverse structures (air columns in dielectric material) with high dielectric constant instead of normal structures [26]. However, the complete PBG may be obtained for normal structure (dielectric column in air background) with lower dielectric contrast ($\varepsilon = 3.8$). **Figure 4** indicates the relations of relative band gap $\Delta\omega/\omega$ with maximum peak value to filling ratio f for different dielectric contrasts. Computations show that the peak value of optimum relative PBG not always augments with the increase of dielectric constant ε for normal structure, instead, the peak value reaches the maximum at about $\varepsilon = 8.9$, such as 9.9% with $f = 15.9\%$ for $\varepsilon = 8.9$ and $c = 1.2$, which is larger than the result (8.8%) of best designed pincushion columns with the same dielectric constant [27]. Specially, in this kind of normal structures, the required minimum permittivity to open a complete photonic band gap with $\Delta\omega/\omega > 1\%$ is near 3.8, which is much lower than the value of 6.4 in the case of pincushion columns [27] and lower than all the results of 2D photonic crystals ever reported before. In addition, the complete PBGs of this

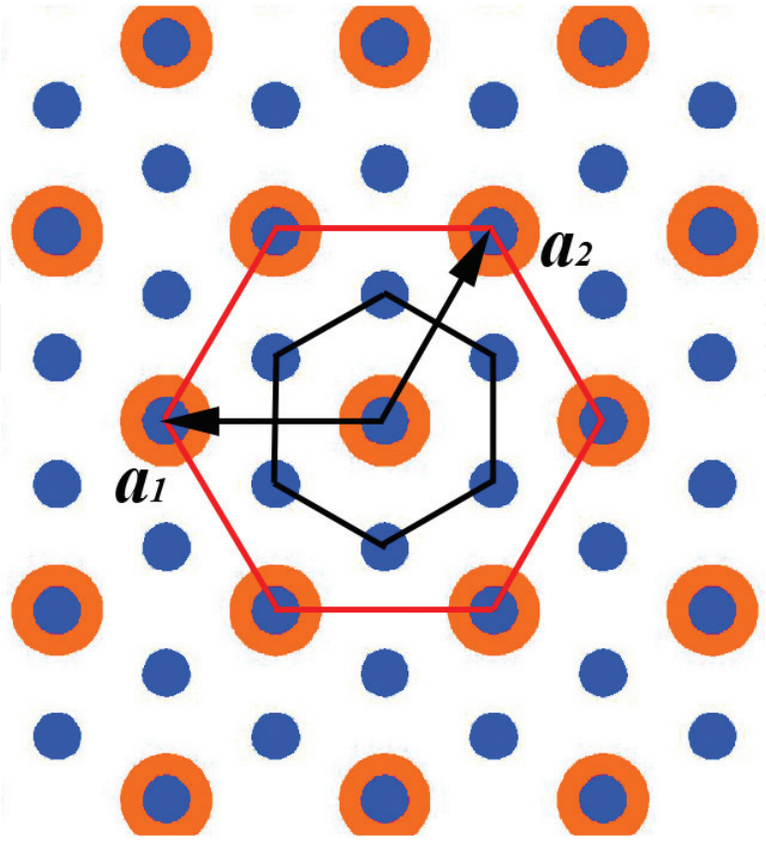

Figure 3. The hybrid triangular lattice, where red dots define triangular sublattice, blue dots define another group with lattice constant $a/\sqrt{3}$ rotated 30°.

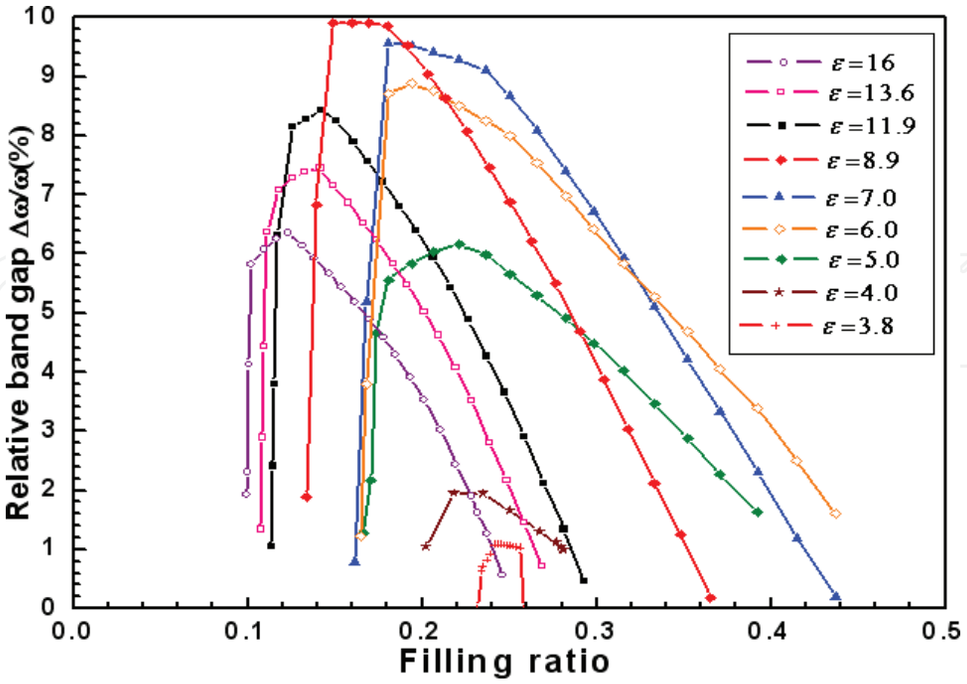

Figure 4. The relations of relative band gaps to different filling ratios *f*.

normal structure exist over wide ranges of coefficient c, filling ratio f and dielectric constant, which can relax the experimental conditions greatly.

2.2. Photonic band gap in 3D-PhCs

An important way to make 3D PhCs by HL is the interference of four umbrellalike beams (IFUB) where three ambient beams (A-beams) form the same apex angle θ with a central beam (C-beam), as shown in **Figure 5** [28, 29]. The possible lattices that IFUB may produce and the polarization optimization in the formation of different lattices have been discussed in the previous works [30, 31]. As a special case of IFUB, the symmetric umbrella configuration, where any two of the three A-beams also form the same angle, is widely used in HL since it can be conveniently realized with the use of a diffraction beam splitter (DBS). The continuous increasing of apex angle θ leads to continuous variation of primitive vectors, reciprocal vectors and the irreducible Brillouin zone of the resultant structure.

The interference of four noncoplanar plane waves of the same frequency will result in an intensity distribution

$$I = I_0 + 2\Delta I(\boldsymbol{r}), \tag{2}$$

where

$$I_0 = \sum_{j=1}^{4} E_j^2, \quad \Delta I(\boldsymbol{r}) = \sum_{i<j} E_i E_j e_{ij} \cos\left[\left(\boldsymbol{K}_i - \boldsymbol{K}_j\right) \cdot \boldsymbol{r} + \phi_{i0} - \phi_{j0} + \sigma_{ij}\right], \tag{3}$$

I_0 is the background intensity, ΔI is the spatial variation of intensity, φ_{j0} is initial phase of the jth wave, $e_{ij} = |\boldsymbol{e}_i \cdot \boldsymbol{e}_j^*|$, and $\sigma_{ij} = \arg(\boldsymbol{e}_i \cdot \boldsymbol{e}_j^*)$. The four wave vectors are expressed as functions of the apex angle θ,

$$\begin{aligned}
\boldsymbol{K}_1 &= (2\pi/\lambda)\left(\left(\sqrt{3}/2\right)\sin\theta, -(1/2)\sin\theta, \cos\theta\right),\\
\boldsymbol{K}_2 &= (2\pi/\lambda)\left(-\left(\sqrt{3}/2\right)\sin\theta, -(1/2)\sin\theta, \cos\theta\right),\\
\boldsymbol{K}_3 &= (2\pi/\lambda)(0, \sin\theta, \cos\theta),\\
\boldsymbol{K}_4 &= (2\pi/\lambda)(0, 0, 1).
\end{aligned} \tag{4}$$

With the angle θ increasing from zero to 180°, the shape of Brillouin zone changes from a small hexangular plane spreading out on xy plane to a simple cubic at $\theta = 70.53°$ and finally to a long hexangular pillar along z axis. **Figure 6** gives the lattice structure and the Brillouin zone calculated at the special angles θ. The special case of $\theta = 38.94°$ corresponds to the fcc structure which belongs to space group No. 166 ($R\bar{3}m$), the structure of $\theta = 109.47°$ is approximate to Schwarz's triply periodic minimal D surface [32].

The plane-wave expansion method [18] was used to study the PBG properties of structures of this kind and search for the corresponding optimum volume filling ratio f yielding maximum relative PBGs. **Figure 7** shows the maximum size of the relative PBG for the optimum filling ratio at different apex angle θ. The complete PBGs exist over a very

http://dx.doi.org/10.5772/intechopen.71403

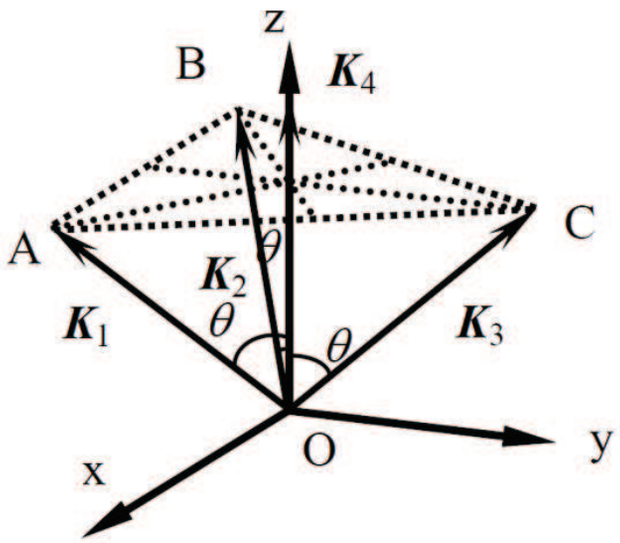

Figure 5. Symmetric umbrella recording geometry and the coordinate system used for calculations.

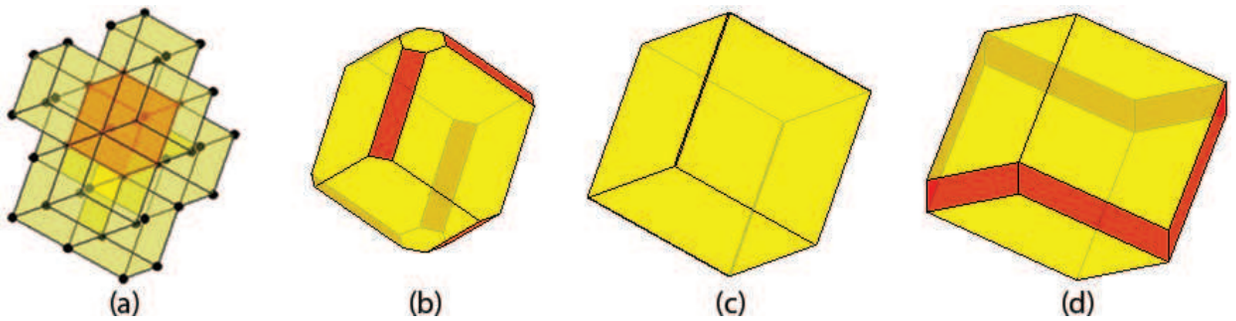

Figure 6. (a) The lattice structure at $\theta = 70.53°$ and (b) the irreducible Brillouin zones of rhombohedral structures for $\theta = 60°$, (c) $\theta = 70.53°$ and (d) $\theta = 80°$.

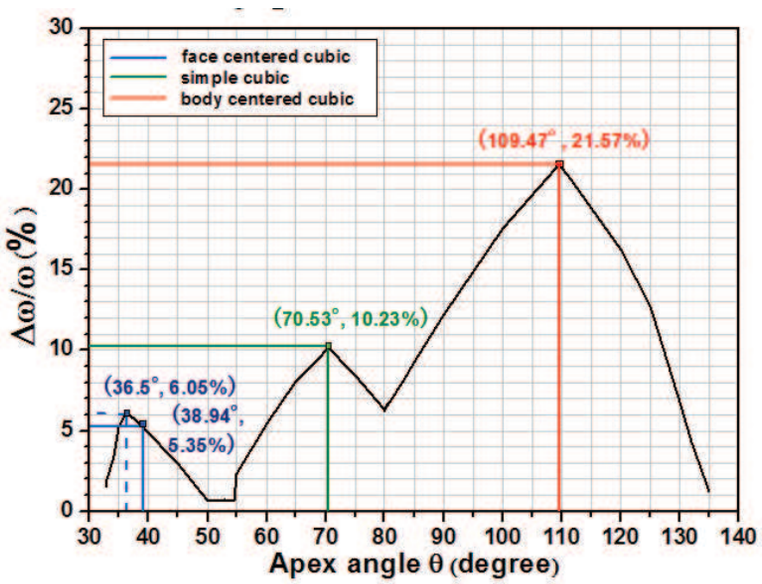

Figure 7. Relative band gap of optimized structures as function of apex angle for $33° < \theta < 135°$ when $\varepsilon = 11.9$.

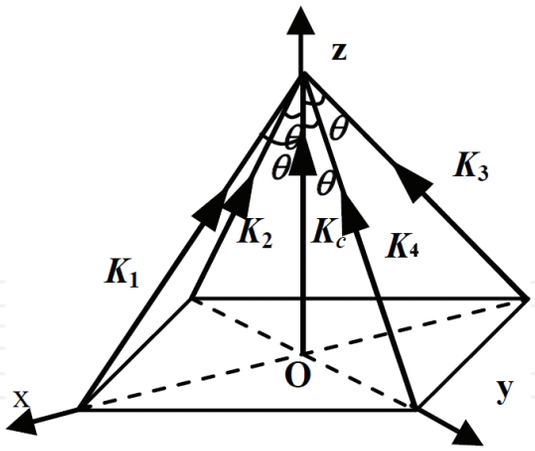

Figure 8. Symmetric umbrella recording geometry and the coordinate system used for calculations.

wide range of apex angle from 33 to 135° except the narrow region from 49 to 55°, and the resultant PBGs of simple cubic-sc, face centered cubic-fcc and body centered cubic-bcc accord with the previous works nicely [32]. The relative PBG width is a continuous function of apex angle with three peaks, and the PBG gradually decreases to zero at θ = 33° and 135°. The first peak of 6.05% corresponds to the rhombohedral structure appears at θ = 36.5°. The second of 10.23% corresponding to the sc structure occurs at θ = 70.53°; and the third one of 21.57% corresponds to the bcc structure at θ = 109.47°.

As mentioned above, the fcc lattice can be obtained by the interference of one central beam and three ambient beams symmetrically scattered around the former, but the structure made in this geometry has only quite a narrow PBG of 5.35%. An alternative beam design was proposed to fabricate the fcc lattice with a large complete PBG, but it requires four beams incident from two opposite surfaces of a sample [33], making it difficult to realize in practice. So a five-beam symmetric umbrella configuration is proposed to make 3D PhCs with large complete PBGs. The proposed recording geometry of five-beam symmetric umbrella configuration is shown in **Figure 8**, where the central beam (C-beam) is set along the z direction, while the four ambient beams (A-beams) are in the *yoz* and *xoz* planes, respectively, to form the same apex angle θ. The above mentioned five wave vectors can be expressed as,

$$\begin{aligned} &\boldsymbol{K}_1 = (2\pi/\lambda)(-\sin\theta,\ 0,\ \cos\theta), \quad \boldsymbol{K}_2 = (2\pi/\lambda)(0,\ \sin\theta,\ \cos\theta), \\ &\boldsymbol{K}_3 = (2\pi/\lambda)(\sin\theta,\ 0,\ \cos\theta), \quad \boldsymbol{K}_4 = (2\pi/\lambda)(0,\ -\sin\theta,\ \cos\theta), \\ &\boldsymbol{K}_c = (2\pi/\lambda)(0,\ 0,\ 1). \end{aligned} \tag{5}$$

This geometry can be realized by using a DBS to obtain a zero-order diffracted beam and four symmetric first-order diffracted beams. The polarization of the central beam is circularly polarized and all the four A-beams are linearly polarized. The unit polarization vectors of five beams are

$$\boldsymbol{e}_1 = \boldsymbol{e}_3 = (0,\ 1,\ 0) \quad , \quad \boldsymbol{e}_2 = \boldsymbol{e}_4 = (1,\ 0,\ 0) \quad , \quad \boldsymbol{e}_c = \frac{1}{\sqrt{2}}(1,\ -i,\ 0), \text{respectively} \tag{6}$$

In general, the lattice structures are tetragonal symmetric structures. The continuous increase of apex angle θ leads to continuous variation of primitive vectors, reciprocal vectors and the

irreducible Brillouin zone of the resultant structure. At $\theta = 70.53°$, the structure is fcc symmetry with respect to diamond structure. Around 70.53°, the lattice is face-centered-tetragonal (fct) symmetry. **Figure 9(a)** and **(b)** show the real fcc structure and its primitive cell fabricated by five-beam symmetric umbrella configuration at $\theta = 70.53°$, which obviously differ from the rhombohedral structure of fcc symmetry and its primitive cell formed by four-beam symmetric umbrella configuration at $\theta = 38.94°$, as shown in **Figure 9(c)** and **(d)**. At the apex angle of $\theta = 90°$, the body-centered-cubic (bcc) lattice can be obtained. For value of θ is near 90°, the structure has body-centered-tetragonal (bct) symmetry.

Full photonic band gaps exist over a very wide range of apex angle with a relatively low refractive index contrast. **Figure 10** represents the relative gap sizes of optimized structures for the apex angle range of $50° < \theta < 115°$ with a dielectric constant contrast of 11.9 to 1 corresponding to silicon in air. It is clear that there are complete PBGs above 10% in the range of $52° < \theta < 112°$, and even larger PBGs above 20% for $59° < \theta < 92°$. The maximum relative gap size of 25.1% appears at $\theta = 70.53°$ corresponding to fcc structure, and the relative gap size of

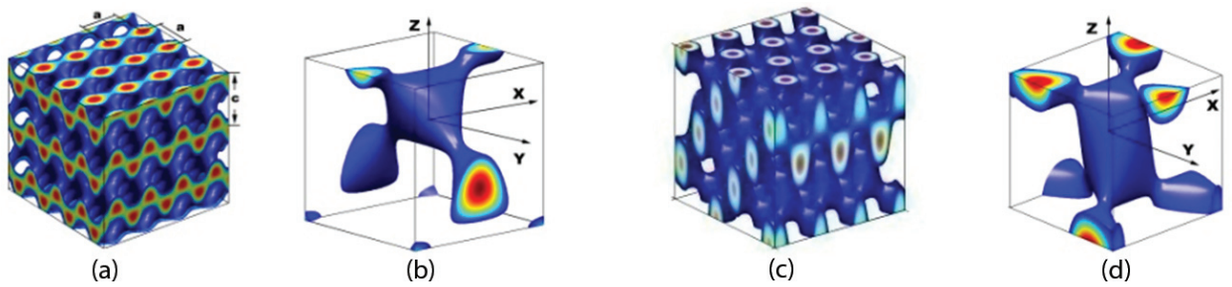

Figure 9. (a) The real fcc structure formed by five-beam symmetric umbrella configuration at $\theta = 70.53°$ and $I_t = 1.39$; (b) the primitive cell of fcc structure; (c) the rhombohedral structure of fcc symmetry constructed by four-beam symmetric umbrella configuration for $\theta = 38.94°$; and (d) the primitive cell of the lattice structure of (c).

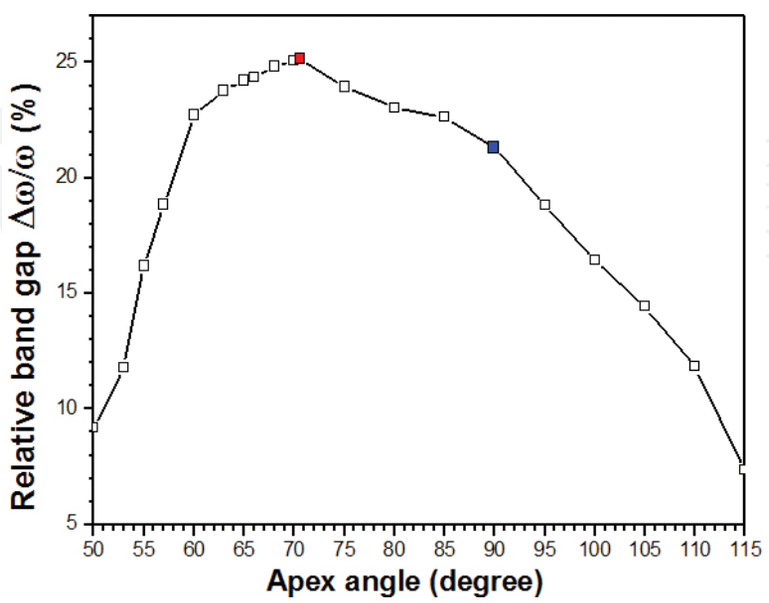

Figure 10. Relative band gap for $50° < \theta < 115°$ when $\varepsilon = 11.9$. The solid symbols are the date for fcc and bcc structures at $\theta = 70.53°$ and 90°, respectively.

bcc structure is 21.3% at $\theta = 90°$. **Figure 11** gives the band structure of the fcc lattice with a large PBG from 0.330 to 0.425$\omega a/2\pi c$ between the second and third bands. Comparing with the four-beam symmetric umbrella configuration, one can find that two results have the similar PBGs of 21.3% for the bcc lattice structures, and the biggest PBG of 25.1% for fcc lattice structure formed by five umbrellalike beams is much larger than the value of 5.35% formed by four umbrellalike beams for the shape reason of PhC lattice cell.

2.3. Photonic crystal waveguide

A waveguide can be created in the PhC slab by introducing a linear defect in the in-plane 2D periodic structure [34, 35]. Since the ability to guide light waves around sharp corners with high efficiency is crucial for photonic integrated circuits, many studies have been carried out concerning waveguide bends through sharp bends in 2D PhC slabs [36, 37]. However, all these works limit the studies to the structures formed by air rods with regular circular cross sections. PBGs for PhCs made by HL may be different from those of regular structures, so will the propagation properties.

When the 2D periodic structure is a triangular Bravais lattice formed by the interference technique of three noncoplanar beams [26], the structure was filled with a material of high refractive index and then removing the template, an inverse structure can be obtained. When the intensity threshold I_t changes from 3.0 to 2.1, the shape of air holes of this inverse structure changes gradually from a circle to a hexagon approximately. a waveguide with two 60° bends are shown in **Figure 12(a)** with the distance between two bends of 9*a*.

Some peaks of transmission may result from the resonance between two bends in the waveguide of ordinary PhCs with circular air holes [38]. The band diagram of the PhC configuration has been calculated with the intensity threshold of $I_t = 2.5$ and filling ratio of $f = 48.7\%$ for the TE-like mode. **Figure 12(b)** indicates the transmission and reflection spectra of the waveguide.

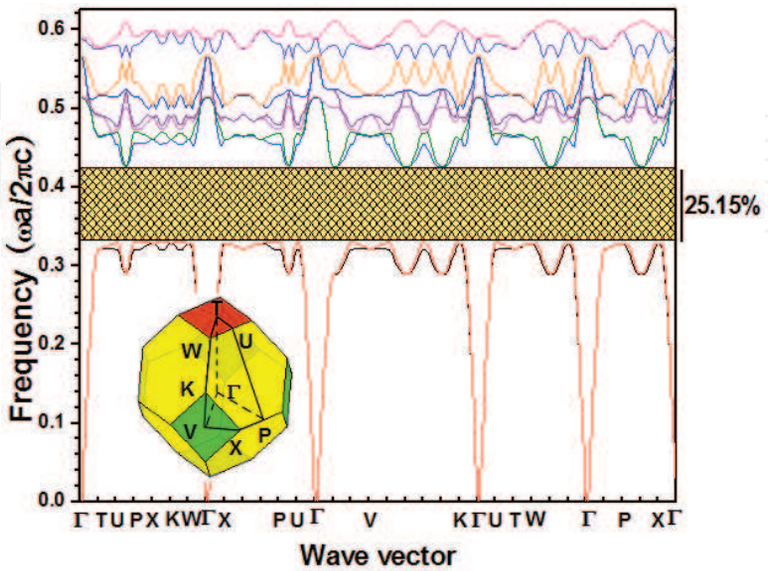

Figure 11. Photonic band structure for the fcc structure with θ = 70.53°. The position of the high symmetry points together with the irreducible Brillouin zone are shown in the inset.

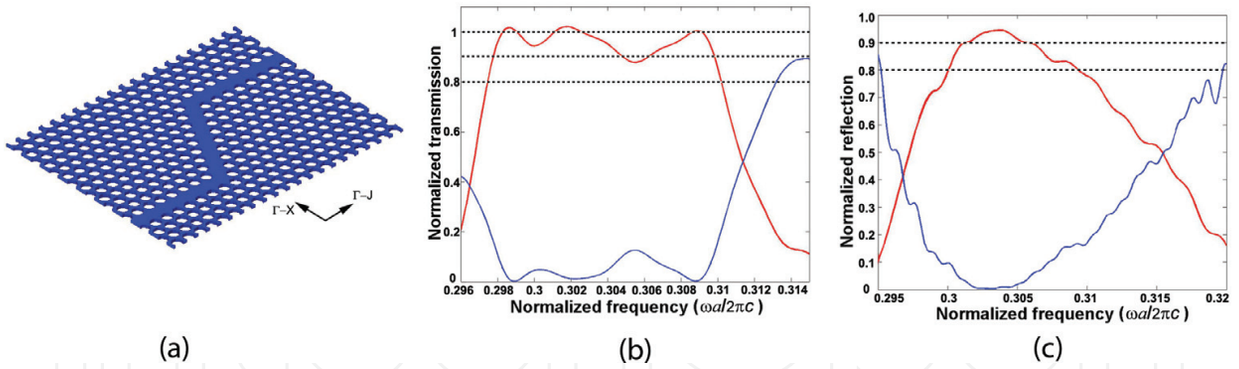

Figure 12. (a) Schematic of a 2D PhC waveguide with two 60° bends and transmission (red curve) and reflection spectra (blue curve) of the PhC waveguide (b) with two bends and (c) one bend.

The red curve here corresponds to the transmission spectra and the blue one to the reflection spectra. High transmission of more than 90% can be obtained in a wide frequency range from 0.298 to 0.310 ($\omega a/2\pi c$). The transmission spectrum of similar PCW with sole 60° bend is shown in **Figure 12(b)**. It is clear that the frequency range of high transmission (>90%) of **Figure 12(b)** is much wider than **Figure 12(c)**. This difference convincingly demonstrates that the existing resonance between two bends induce strong effect on the transmission property of the PCW, which can be used to optimize the PCW design effectively.

Different from the total internal reflection and photonic crystal fibers (PCF) with full 2D PBGs by introducing line defect, a 2D photonic crystal waveguide (PCW) formed by an air core and two identical semi-infinite layers of left-handed holographic PhC is proposed to confine light in air waveguide. As shown in **Figure 13**, The EFCs plot and wave-vector diagram of TM2 band in the HL photonic crystal indicate the PhC is left-handed. Considering the symmetry of Bloch modes of this PhC, the incident interface can be placed in ΓM or ΓK directions. Simulations have demonstrated that the incident beam can readily travel through the PhC slab with the input surface interface normal to ΓM direction, but restrained in ΓK direction, which may originate from the symmetry mismatch between the external incident wave and the Bloch mode of this PhC structure [39].

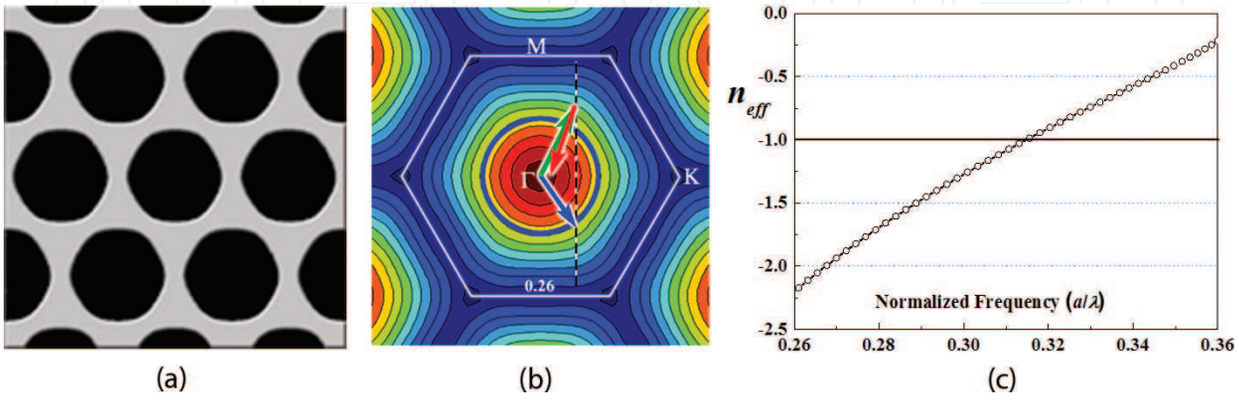

Figure 13. (a) The dielectric pattern of cross section with $I_t = 2.33$; (b) EFC plot and wave-vector diagram of TM2 band; (c) effective index of TM2 band vs. the normalized frequency.

An air waveguide is introduced in the PhC along ΓK direction, as shown in **Figure 14(a)**, with the length 50*a* of PCW. The power flow can become negative in the PhC cladding when $\varepsilon_x < 0$, but remain positive in the air core. By reducing the air width to a critical thickness for TM mode at certain frequency, the group velocity decreases to zero due to the energy flow in the air core was offset by the energy flow of the PhC cladding [39]. According to the result of Ref. [40] the wave vector of guided waves can be given by $k_z = m\pi/d$ with $m = 1,2,\ldots$, and the guided waves can pass through the super waveguide composed of one air layer and LHM for the width of air waveguide $d > \lambda_0/2$ (λ_0 is the wavelength in air). The larger d is, the more modes are guided in the super waveguide. To satisfy the guided condition the width of air layer d is chosen to be equal or greater than that of 2 layers. A Gaussian pulse with the frequency spanning from 0.26 to 0.38 is excited at the input (left) side of the waveguide to investigate the transmission properties of this holographic PCW. The transmission spectrums of different widths of air waveguides are shown in **Figure 14(b)**. Obviously, a high transmission (>90%) happened in the frequency regime from 0.315 to 0.365 through the air waveguide with the width of 4 layers, corresponding to $0 < |n_{eff}| < 1$, which verifies the oscillating modes has a real propagation constant [40]. With the width of air waveguide reducing from 4 to 2 layers, the group velocities decrease gradually and backscattering loss becomes the dominant factor [41], the critical excitation frequency changes from 0.315 to 0.334 and the transmittance decreases gradually for the backscattering loss weakening the guided Bloch mode.

Figure 15 shows TM field in the waveguide with 3 layers of air width for the cases when frequencies are (a) 0.28, (b) 0.315 and (c) 0.33 respectively, light attenuation can be seen clearly in **Figure 15(a)** as a result of vertical scattering loss. Since air thickness decreases from 4 layers to 3 layers, the group velocities slow down and the backscattering loss becomes a dominant loss factor. The light with the frequency of 0.315 display a low transmission in the waveguide as shown in **Figure 15(b)**. **Figure 15(c)** verifies that the incident wave with frequency beyond the minimum critical excitation frequency can be well confined to the air waveguide. Based on the symmetry mismatch between the incident wave and the Bloch modes of the holographic PhC, a holographic PCW without PBGs can also efficiently guide light in a wide frequency region with high transmission efficiency.

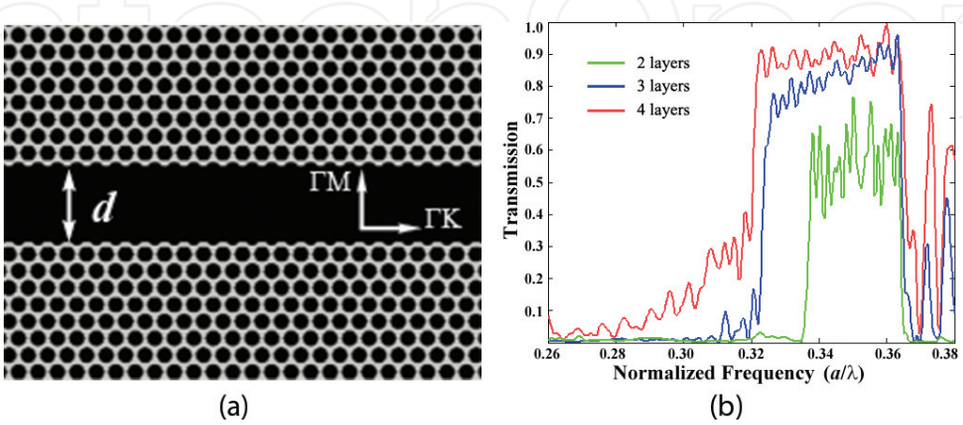

Figure 14. (a) Schematic of the holographic PhC waveguide with a 4 layers width; (b) variation of transmission spectrum for the holographic PCW with different air width.

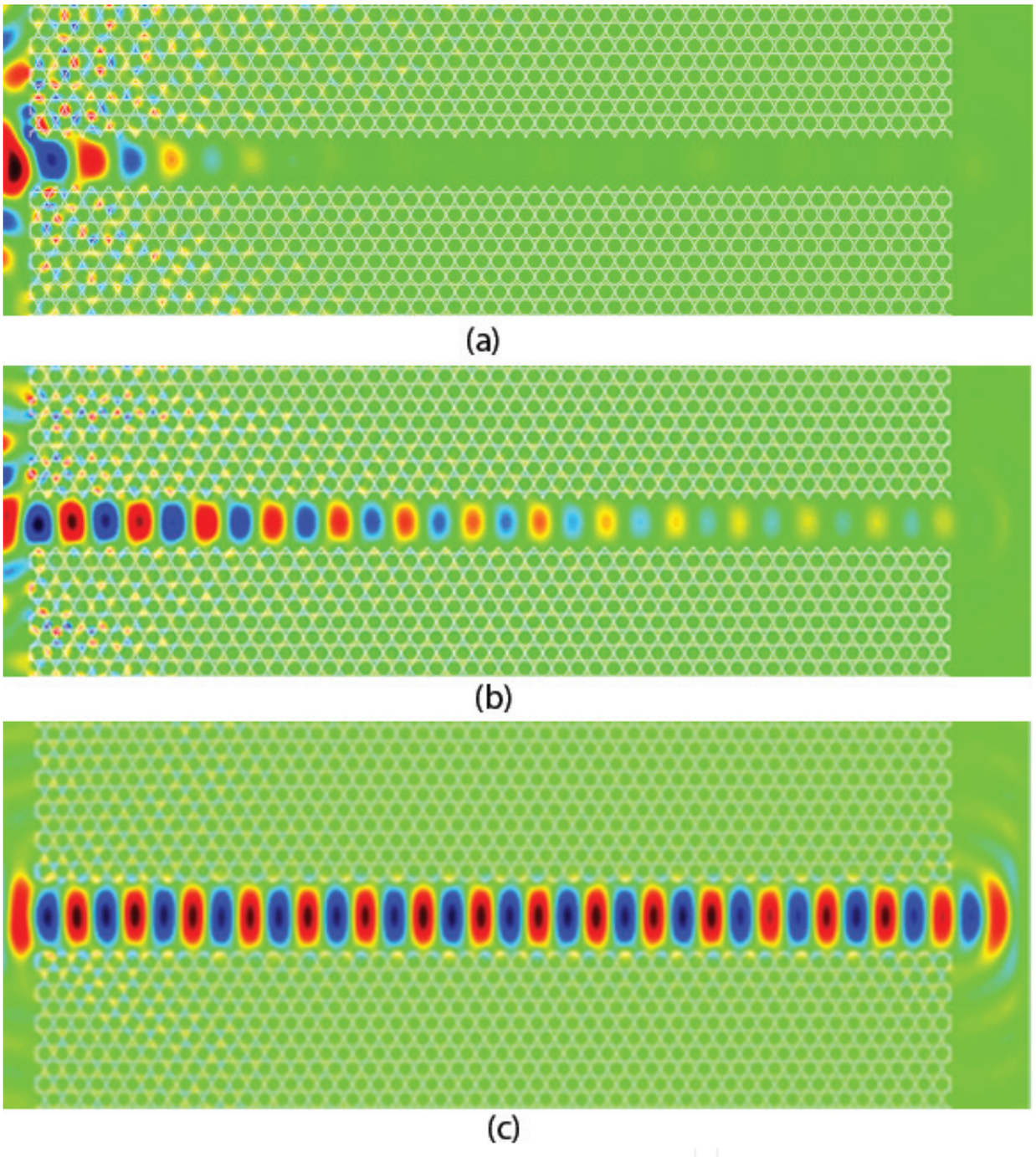

Figure 15. Snapshots of the propagations of TM polarization monochromatic wave at the frequencies of (a) 0.28, (b) 0.315 and (c) 0.33 in the holographic PCW of I_t = 2.33 with 3 layers width.

3. Anomalous refraction behaviors modulated by PhC bands

Photonic crystals can exhibit an extraordinarily high, nonlinear dispersion such as negative refraction and self-focusing properties that are solely determined by the characteristics of their band structures and equal frequency contours (EFC) [42–44]. The 2D honeycomb structures

formed by single-exposure interference fabrication methods is used to investigate a series of HL PhC structures in order to obtain comprehensive understanding of the anomalous refractive properties in PhCs.

The filling ratio of the HL PhC is determined by the ratio of the total exposure dose. Silicon with $\varepsilon = 11.56$ (i.e., n = 3.4) is used to analyze the dispersion characteristics of the holographic PhCs. **Figure 16(a)** gives the cross section of the HL PhC sample. The EFCs plot and wave-vector diagram of TM2 band in **Figure 16(b)** illustrated the EFCs around point Γ are convex and shrink with increasing frequency, indicating the PhC is left-handed. Due to the symmetry mismatch between the external plane wave at normal incidence and the Bloch modes of this PhC as mentioned above, the interface between PhC and free space is arranged along the ΓK direction.

As shown in **Figure 16(a)**, the surface of dielectric PhC slab with the trigonal flange (cut $0.4a$) was disposed to reduce the reflection and scattering losses effectively [45], because of the effective index gradually varying to match with free space. A continuous monochromatic TM polarization plane wave at the desired frequency $\omega = 0.348$ incidents on the PhC slab with the incident angles of $\theta = 30^\circ$ and 60°. The wave patterns are shown in **Figure 16(c)** and **(d)**, respectively, with the refracted beams and incident beams symmetrically located on the same side of normals, which illustrate the effective refractive index of this PhC is $n_{\text{eff}} = -1$, and the phenomenon of negative refraction in this PhC is an absolute left-handed behavior with $\boldsymbol{K}_{\text{r}} \cdot \boldsymbol{V}_{\text{gr}} < 0$.

For a continuous point source of $\omega = 0.348$ located on the upper side of the PhC slab with the distance of $d_{\text{o1}} = 8.0a$ away from the upper interface (i.e., the object distance), as shown in **Figure 17(a)**, the image point approximately locates at the edge of the lower surface with the image distance $d_{\text{i1}} = 0$. In **Figure 17(b)**, the relevant image distance becomes $d_{\text{i2}} \approx 4.6a$ for the object distance of $d_{\text{o2}} = 3.5a$. Obviously, the sum of d_{o} and d_{i} in this PhC slab is nearly a constant and satisfies the Snell's law of a flat lens with $n_{\text{eff}} = 1$. In addition, note that there is an internal focus inside the PhC slab of **Figure 17(b)**, which is a clear evidence of LHMs following the geometric optics rules.

Multi-refraction effects in the 2D triangular PhC have also been found [43]. The special EFC distributions of different bands can be used to predicate the propagating properties of incident electromagnetic wave (EMW). The EFC plot of the second band is shown in **Figure 18(a)** with almost straight EFC in the ΓK direction at the frequency of 0.26 a/λ. The group velocity v_{gr} of refracted waves ought to be perpendicular to the incident surface among the incident angle region from 0 to 35°, which have been demonstrated by the simulation results in **Figure 18(b)–(d)**. This unusual collimation effect has a series of exciting potential applications, such as spatial light modulator and optical collimator.

The k-conservation relation is observed in wave-vector diagrams [44]. Traditional EMWs propagate in media with their wavefronts perpendicular to the energy flow direction. Here, the EMW of 0.36 a/λ incident upon the ΓK surface at $\theta_{inc} = 25^\circ$, the wavefronts of refracted wave are modulated by the periodic PhC to parallel to the energy flow direction with $\boldsymbol{k} \cdot \boldsymbol{v}_{gr} = 0$. **Figure 19(a)** gives the analysis of EFC plot and wave-vector diagram. FDTD simulations of electric field distribution in **Figure 19(b)** prove with the certainty of theory analysis results with the parallel wavefronts extending along the transmission line.

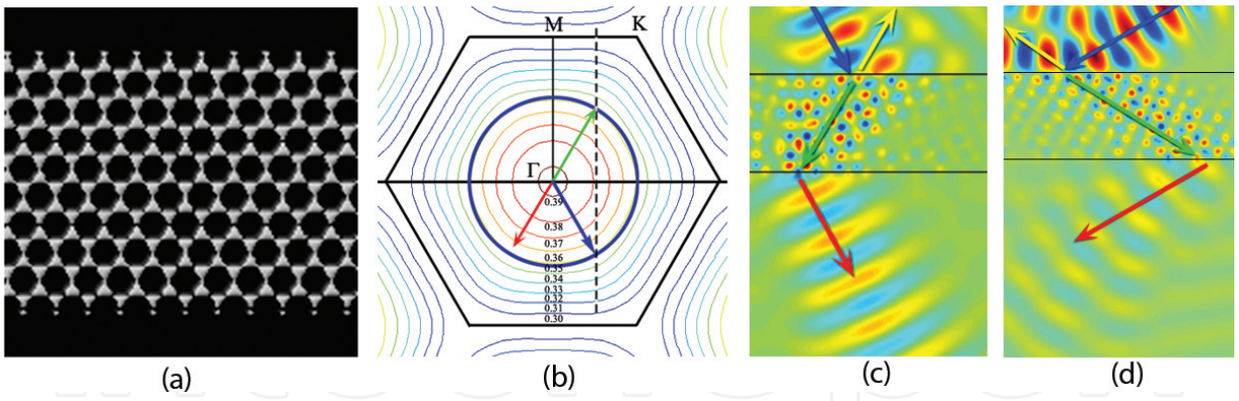

Figure 16. (a) Schematic view of the HL PhC slab with the trigonal dielectric flange; and (b) the wave patterns of negative refractions for different incident angles of (c) $\theta = 30^\circ$ and (d) $\theta = 60^\circ$.

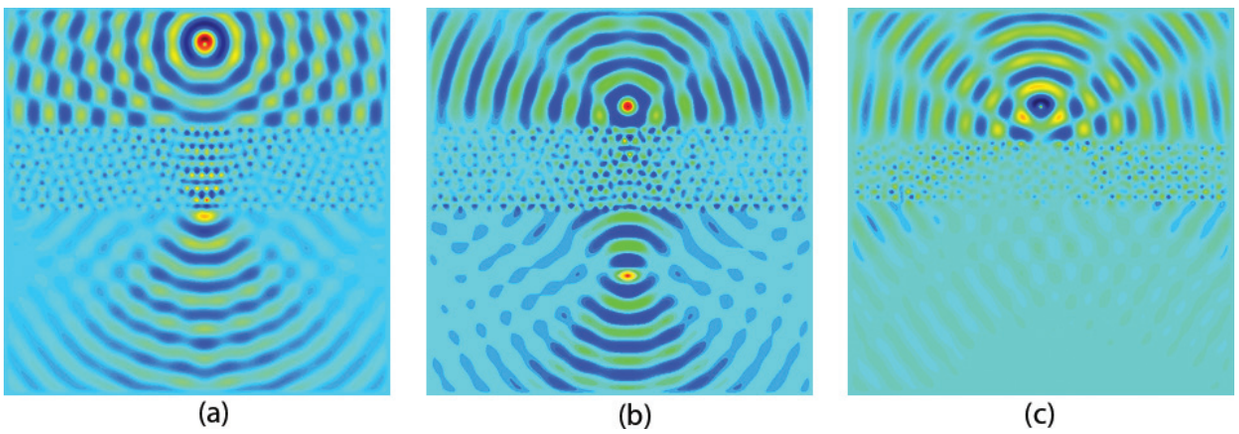

Figure 17. Field patterns for the flat superlens. The object distance is 8.5*a* (a) and 3.5*a* (b) for the interface normal to ΓM direction, and (c) 3.5*a* for the interface normal to ΓK direction.

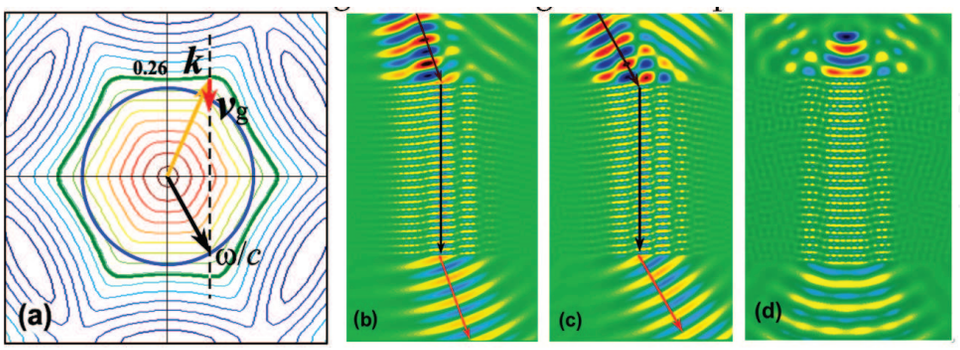

Figure 18. (a) EFC plot of the second band with the wave-vector diagrams at 0.26a/λ and the FDTD simulations of electric field distributions with different incident angles of (b) 20°, (c) 30° and (d) point source incident.

For the normal HL structure with triangular lattice symmetry of $I_t = 1.90$ (or $f = 82.8\%$), the EFC plots of TM2 and TM3 bands are calculated [46]. Different from the EFCs of inverse HL structure, TM2 and TM3 bands intersect in the frequencies regime from 0.225 to 0.343.

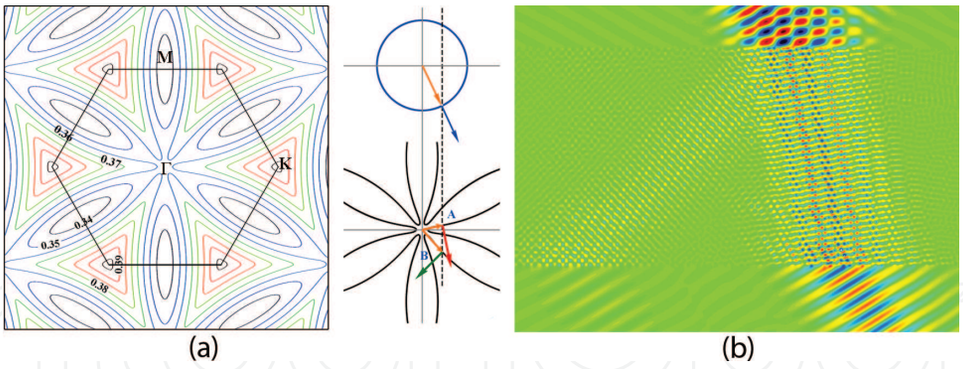

Figure 19. (a) EFC plot of the fourth band and wave-vector diagram at 0.36a/λ with θ_{inc} = 25°; (b) the FDTD simulations of electric field distributions.

When a Gaussian beam of ω = 0.31 incidents on the ΓK surface at θ = 25°, the wave-vector diagram is shown in **Figure 20(a)** with the blue circle representing the EFC in air, the brown ring denoting the EFC of TM2 band, and the green hexagram corresponding to the EFC of TM3 band. Obviously, the dashed conservation line intersects with EFCs of TM2 and TM3 simultaneously to excite two beams of left-handed negative refraction with different refractive angles, because of the unique EFC features, as shown in **Figure 20(b)** to verify this result.

The more complicated refraction behaviors can be excited in the higher band regions based on the intricate undulation of one band or the overlap of different bands. As shown in **Figure 21(a)**, the sixth band has dual parallel EFCs with opposite curvatures by the red rings within the frequency range from 0.44 to 0.47 a/λ within a wide scope of incident angle. As an example, when the working frequency is chosen to be 0.46a/λ, the incident wave at θ_{inc} = 30° can excite positive and negative refracted waves have the symmetrical refractive angles of ±30°. The seventh band has more frequency undulations circled by the blue rings which lead to the more intricate triple refraction within the frequency scope from 0.488 to 0.50 a/λ (**Figure 21(b)**).

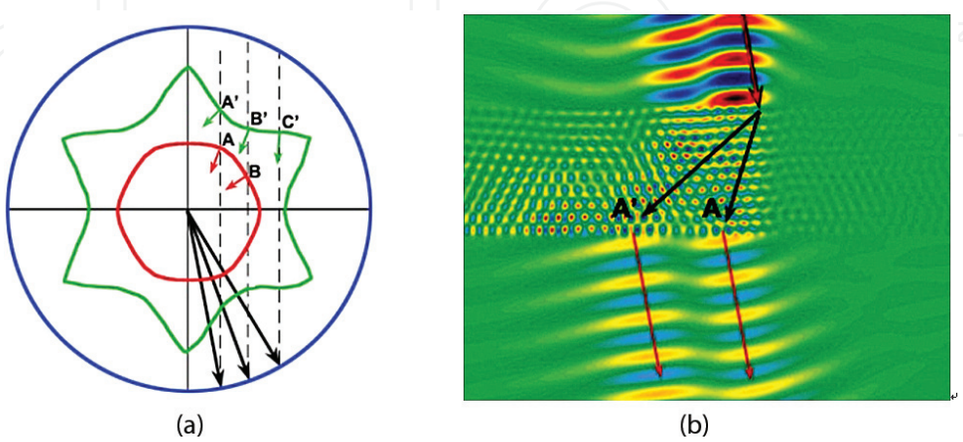

Figure 20. (a) Wave-vector diagram of ω = 0.31 for TM2 (brown ring) and TM3 (green hexagram); (b) field pattern with the incident beam of ω = 0.31 at the incident angle of 25°.

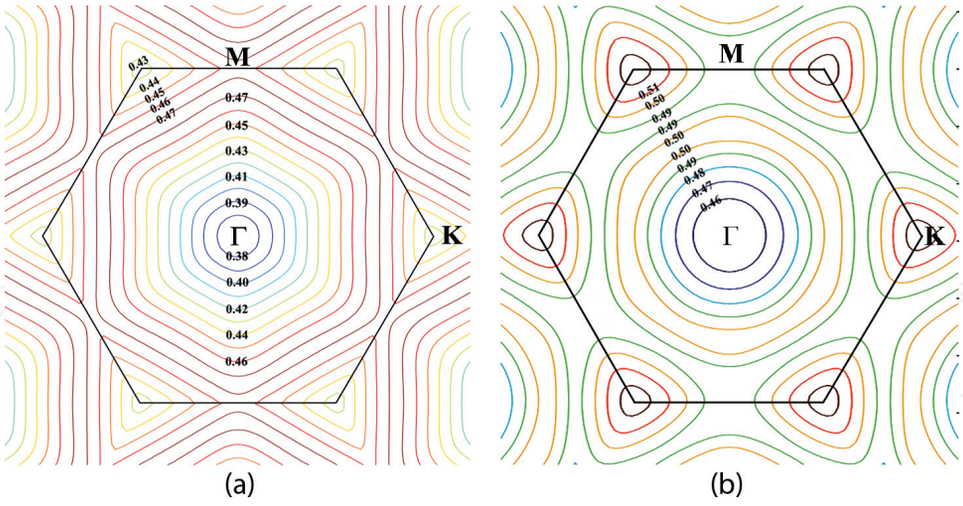

Figure 21. EFC plots of (a) the sixth band and (b) the seventh band.

4. Phenomena of zero phase delay in PhCs and application

Recently, materials with zero or near-zero-n has attracted great focus for the characteristics of uniform phase and infinite wavelength [47–50]. A series of exciting potential applications have been found in zero-n materials, such as wavefront reshaping [51], beam self-collimation [52], extremely convergent lenses [53], etc. One of their best known applications is optical links in lumped nanophotonic circuits over hundreds of wavelengths without introducing phase shifts so as to reduce the unwanted frequency dispersion. Different strategies have been provided to realize zero permittivity ε. One is to use metallic metamaterial structures with effective zero permittivity and/or permeability [54, 55]. However, these metamaterials suffer from the strong absorption loss of the metals and hence with greatly deteriorated transmittance. Some alternative approaches have been provided, include the combination of negative- and positive-index materials [52], the microwave waveguides below cutoff [56] or the periodic superlattice formed by positive index homogeneous dielectric media and negative index photonic crystals (PhCs) [57].

A plane wave can be described as $\tilde{E}(\boldsymbol{r}) = A\exp\left[i\left(\boldsymbol{k}\cdot\boldsymbol{r}+\varphi_0\right)\right]$, where the symbols of A, $\boldsymbol{k}$, $\boldsymbol{r}$, ϕ_0 denote wave amplitude, wave vector, position vector and initial phase. The spatial phase shift is determined by the spatial phase factor $\boldsymbol{k}\cdot\boldsymbol{r}$, with the traditional wave vector $\boldsymbol{k}$ pointing to the direction of energy flow (i.e. the direction of group velocity $\boldsymbol{v}_{gr}$). Assuming the condition of $\boldsymbol{k}\cdot\boldsymbol{r}=0$ is satisfied, the wave vector $\boldsymbol{k}$ is perpendicular to the energy flow with the wavefronts extending along the propagation direction with the stationary spatial phase along the direction of energy flow $\boldsymbol{S}$. In general, it is difficult to modulate the direction of wavefronts in homogeneous materials. Since this formula of $\boldsymbol{k}\cdot\boldsymbol{r}=0$ can also be expressed as $\boldsymbol{k}\cdot\boldsymbol{v}_{gr}=0$, by the definition of group velocity $\boldsymbol{v}_{gr}=\nabla_{\boldsymbol{k}}\omega$ in PhCs, the group velocity vector is perpendicular to EFCs pointing to the frequency-increasing direction. Hence, by adjusting the EFC distribution, the condition of zero phase delay with $\boldsymbol{k}\cdot\boldsymbol{r}=0$ can be satisfied.

The PhC sample of triangular lattice is composed of dielectric rods with ε_r = 10, diameter d = 10 mm, height h = 10 mm and lattice constant a = 10 mm. When the beam of the frequency ω = 0.376 is incident upon the ΓK surface with the incident angle of θ_{inc} = 30°. The wave-vector diagram of the fourth band is shown in **Figure 22**. According to the condition of boundary conservation, two refracted waves can be excited in the PhC. The condition of $\boldsymbol{k} \cdot \boldsymbol{r} = 0$ is satisfied for the positive refracted wave. Simulations and experiments in a near-field scanning system have demonstrated that the wavefronts exactly are parallel to the energy flow with zero phase delay, as shown in **Figure 23(a)** and **(b)**. The measured phase contrast image is shown in **Figure 23(c)** at 11.213 GHz. Obviously, the incident wave and the exit wave can be connected directly as if the PhC slab did not exist. Since the PhC structure can be engineered readily with the large design flexibility, the frequency and incident angle of zero phase delay can be adjustable in a relaxed PhC configuration design.

Another approach to realize zero phase delay in PhCs is based on the accidental degeneracy of two dipolar modes and a single monopole mode generates at the Dirac-like point (DLP) with the linear dispersions of Dirac cone at the Brillouin zone center of PhCs [58]. At the DLP shown in **Figure 24(a)**, the PhC can mimic the zero-index medium (ZIM) with the characteristics of uniform field distribution. Linear dispersions near the center point induced by the triple degeneracy display many unique scattering properties, such as conical diffraction [59], wave shaping and cloaking [60]. The dispersion properties obeying the 1/L scaling law near the DLP in the normal propagation direction have been verified theoretically and experimentally [61] through the dielectric PhC ribbons with the finite thicknesses, however, it is difficult to distinguish the precise crossing point from the wide extremum range just relying on the transmittance spectrum.

A Gaussian pulse source of TM mode was placed in front of a PhC square-lattice array with the incident angle of 90°, thus three transmission spectrums can be measured outside the other three output interface of the PhC array with one in parallel direction and two in perpendicular upward and downward directions. As long as the size is large enough, the PhC array can be

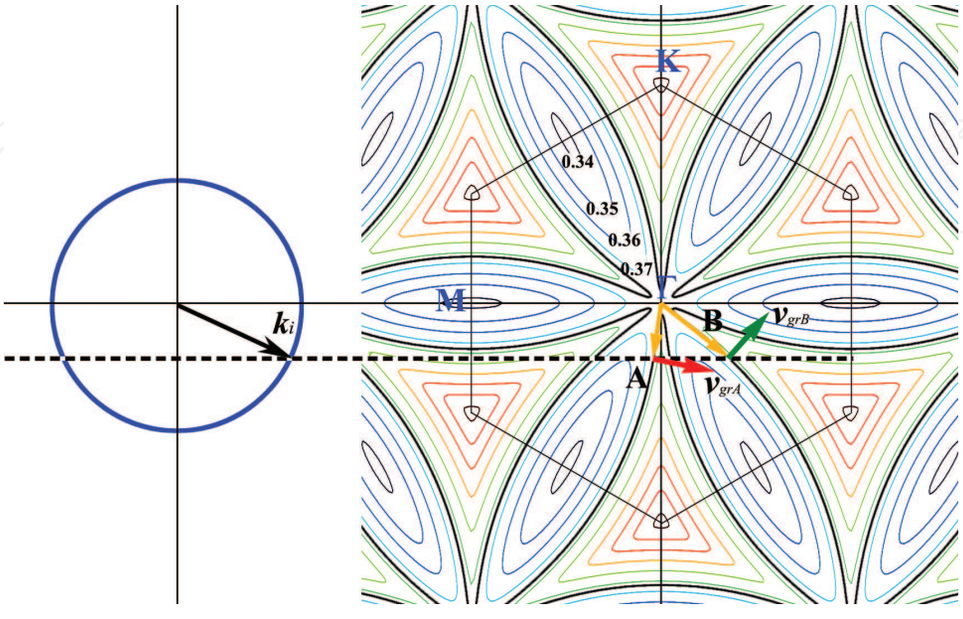

Figure 22. EFCs plot of the fourth band with the wave-vector diagram at $\omega = 0.376a/\lambda$ with θ_{inc} = 30°.

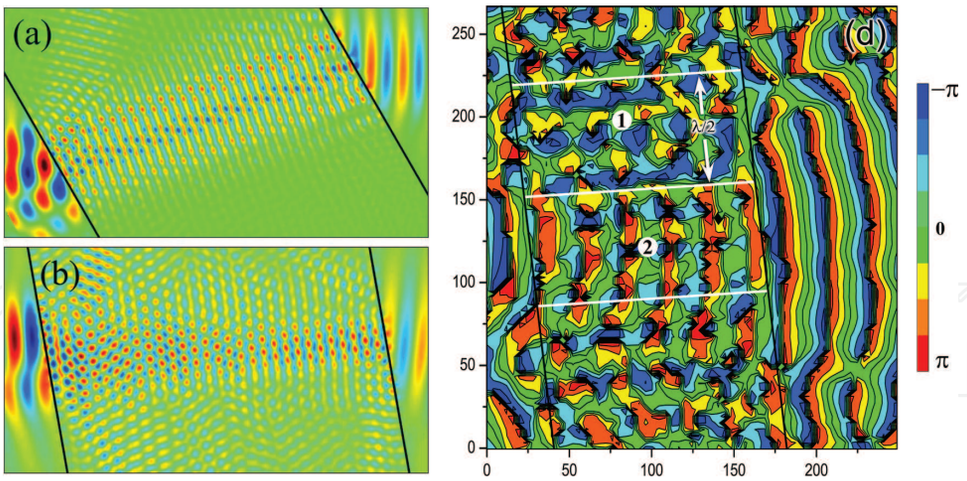

Figure 23. (a, b) Wavefront distribution in the PhC slab with different incident angles; (c) measured phase contrast image.

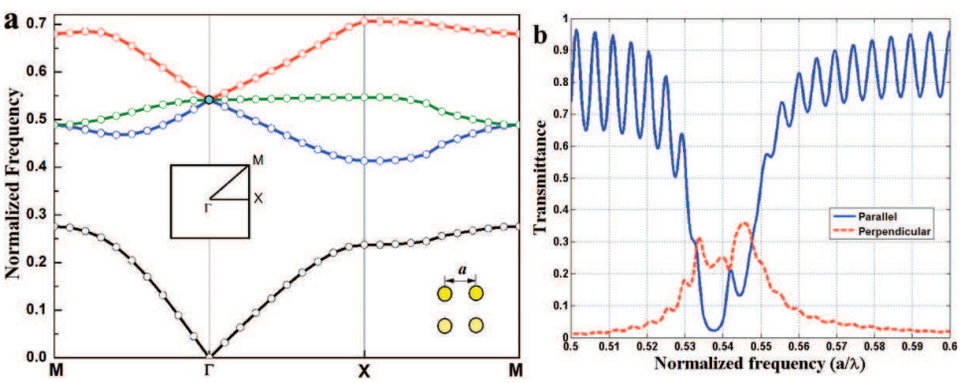

Figure 24. (a) Band structure of TM waves for the 2D square-lattice PhC at the normalized frequency $\omega_D = 0.541$. (b) The simulated transmission spectra in the directions parallel and perpendicular to the incident propagation direction.

regarded as an infinite PhC with the similar transmittance at the different exit boundaries with the same interface structure. As shown in **Figure 24(b)**, the upward and downward sharp cusps embedded in the parallel and perpendicular extremum transmittance spectra intersect at the DLP frequency, therefore, the DLP can be identified accurately due to the property of uniform field distribution of PhC with effective zero index at DLP.

5. Conclusion

In summary, some novel kinds of 3- and 2-D lattices formed by holographic lithography have been investigated to find that the complete PBG over wide ranges of system parameters can be achieved by proper design. The beam design for making this structure is also derived. By using the interference of symmetric four umbrellalike beams one can obtain complete PBGs over a very wide range of apex angle, three special lattice structures of fcc, sc and bcc were achieved with different complete PBGs of 5.35%, 10.23% and 21.57%. The similar PBG of 21.3% for the bcc lattice structures, and the biggest PBG of 25.1% for fcc lattice structure were achieved by five

umbrellalike beams, which is much larger than the value of 5.35% formed by four umbrellalike beams for the shape reason of PhC lattice cell. The holographic PCW can efficiently guide light in a wide range of frequency around sharp corners and the resonance between the two bends has a close relation with the configuration of PhC which can be regarded as an important factor to improve the transmission property of 2D PCW. Since the absolute refractive index 1 of the air guiding core is larger than the effective index of PhC cladding, the total internal reflections can be achieved approximately with a high transmittance in the PhC waveguide with the effective refraction index near zero. For PhC waveguide when the width of air layer is greater than the critical thickness, the problems of scattering loss can be avoided. The proposed left-handed holographic PCW is more suitable for many applications in the area of photonic integrated circuits, and the idea and method of analysis here open a new freedom for PCW engineering.

Different from the anomalous phenomena of PhCs in the high bands, the PhCs of honeycomb-lattice in the lower band region are more suitable to realize the effect of all-angle left-handed negative refraction. For the straight EFCs distribution in special directions, the regular PhC can be applied to the design of optical collimator. Moreover, multi-refraction has been found in the higher bands. There are two ways to realize multi-refractions, one arises from a single band with intricate undulations and another originates from the overlap of multi-bands. The unique phenomena of dual-negative refraction and positive-negative refraction have been found in the higher bands of PhC. Based on the design flexibility of PhC, the transmission properties of PhC can be engineered with a large freedom. These results are important and useful for the design of PhC device.

An efficient way to achieve EMW propagation with zero phase delay is to modulate the wavefronts paralleling to the direction of energy flow. This method can be extended from 2D to 3D cases or other artificially engineered materials, which opens a new door to obtain perfect zero-phase-delay propagation of EMW and has significant potential in many applications. Furthermore, the research found that the Dirac-like point of PhC can be identified accurately by measuring the transmission spectra through a finite photonic crystal square array.

All these results can be extended to the fabrication of other artificially engineered materials and provide guidelines to the design of new type optical devices.

Acknowledgements

This work was supported by National Natural Science Foundation of China (11574311, 51532004, 61275014)

Author details

Guoyan Dong

Address all correspondence to: gydong@ucas.ac.cn

College of Materials Science and Opto-Electronic Technology, University of Chinese Academy of Sciences, Beijing, China

References

[1] Yablonovitch E. Inhibited spontaneous emission in solid-state physics and electronics. Physical Review Letters. 1987;**58**:2059. DOI: 10.1103/PhysRevLett.58.2059

[2] Joannopoulos JD. et al. Photonic Crystals: Molding the Flow of Light. NJ, USA: Princeton University Press; 2008. DOI: 10.1016/S0038-1098(96)00716-8

[3] Johnson S, Villeneuve P, Fan S, Joannopoulos J. Linear waveguides in photonic-crystal slabs. Physical Review B. 2000;**62**:8212-8222. DOI: 10.1103/PhysRevB.62.8212

[4] Mekis A, Chen J, Kurland I, Fan S, Villeneuve P, Joannopoulos J. High transmission through sharp bends in photonic crystal waveguides. Physical Review Letters. 1996;**77**:3787. DOI: 10.1103/PhysRevLett.77.3787

[5] Krauss T, Rue R, Brand S. Two-dimensional photonic-bandgap structures operating at near-infrared wavelengths. Nature. 1996;**383**:699-702. DOI: 10.1038/383699a0

[6] Zhang X, Jackson T, Lafond E, Deymier P, Vasseur J. Evidence of surface acoustic wave band gaps in the phononic crystals created on thin plates. Applied Physics Letters. 2006;**88**:041911. DOI: 10.1063/1.2167794

[7] Aoki K, Miyazaki H, Hirayama H, Inoshita K, Baba T, Sakoda K, Shinya N, Aoyagi Y. Microassembly of semiconductor three-dimensional photonic crystals. Nature Materials. 2003;**2**:117-121. DOI: 10.1038/nmat802

[8] Moroz A. Three-dimensional complete photonic-band-gap structures in the visible. Physical Review Letters. 1999;**83**:5274-5277. DOI: 10.1103/PhysRevLett.83.5274

[9] Liu K, Avouris P, Bucchignano J, Martel R, Sun S, Michl J. Simple fabrication scheme for sub-10 nm electrode gaps using electron-beam lithography. Applied Physics Letters. 2002;**80**:865-867. DOI: 10.1063/1.1436275

[10] Farsari M, Vamvakaki M, Chichkov B. Multiphoton polymerization of hybrid materials. Journal of Optics. 2010;**12**:124001. DOI: 10.1088/2040-8978/12/12/124001

[11] Miklyaev Y, Meisel D, Blanco A, Freymann G. Three-dimensional face-centered-cubic photonic crystal templates by laser holography: Fabrication, optical characterization, and band-structure calculations. Applied Physics Letters. 2003;**82**:1284-1286. DOI: 10.1063/1.1557328

[12] Veselago V, Lebedev P. The electrodynamics of substances with simultaneously negative values of ε and μ. Soviet Physics Uspekhi. 1968;**10**:509-514. DOI: 10.1070/PU1968v010n04ABEH003699

[13] Ziolkowski R, Heyman E. Wave propagation in media having negative permittivity and permeability. Physical Review E. 2001;**64**:056625. DOI: 10.1103/PhysRevE.64.056625

[14] Lindell I, Tretyakov S, Nikoskinen K, Ilvonen S. BW media—media with negative parameters, capable of supporting backward waves. Microwave & Optical Technology Letters. 2001;**31**:129-133. DOI: 10.1002/mop.1378

[15] Shelby R, Smith D, Schultz S. Experimental verification of a negative index of refraction. Science. 2001;**292**:77-79. DOI: 10.1126/science.1058847

[16] Rakich P, Dahlem M, Tandon S, et al. Achieving centimetre-scale supercollimation in a large-area two-dimensional photonic crystal. Nature Materials. 2006;**5**:93. DOI: 10.1038/005093a0

[17] Vasić B, Gajić R. Self-focusing media using graded photonic crystals: Focusing, Fourier transforming and imaging, directive emission, and directional cloaking. Journal of Applied Physics. 2011;**110**:1771-1180. DOI: 10.1063/1.3630116

[18] Cao Y, Hou Z, Liu Y. Convergence problem of plane-wave expansion method for phononic crystals. Physics Letters A. 2004;**327**:247-253. DOI: 10.1016/j.physleta.2004.05.030

[19] Bondeson A, Rylander T, Ingelström P. The finite-difference time-domain method. In: Computational Electromagnetics. Vol. 51. New York, NY: Springer; 2001. pp. 57-86. DOI: 10.1007/0-387-26160-5_5

[20] Dong G, Yang X, Cai L, Shen X, Meng X, Xu X, Wang Y. Band gap analysis and holographic design of 3-fold hybrid triangular photonic crystals of irregular columns with large full band gaps. Journal of Optics A: Pure and Applied Optics. 2007;**9**:531. DOI: 10.1088/1464-4258/9/5/017

[21] Dong G, Yang X, Cai L, Shen X, Meng X, Xu X, Zhang H. Six-fold hybrid photonic crystal formed holographically with full band gap for low refractive index. EPL. 2007;**80**:14006. DOI: 10.1209/0295-5075/80/14006

[22] Cai L, Dong G, Feng C, Yang X, Shen X, Meng X. Holographic design of a two-dimensional photonic crystal of square lattice with a large two-dimensional complete bandgap. Journal of the Optical Society of America B. 2006;**23**:1708-1711. DOI: 10.1364/JOSAB.23.001708

[23] Joannopoulos J, Villeneuve P, Fan S. Erratum: Photonic crystals: Putting a new twist on light. Nature. 1997;**386**:143-149. DOI: 10.1038/386143a0

[24] Russell P. Photonic crystal fibers. Science. 2003;**299**:358. DOI: 10.1126/science.1079280

[25] Sharp D, Campbell M, Dedman E, Harrison M, Denning R, Turberfield A. Photonic crystals for the visible spectrum by holographic lithography. Nature. 2000;**404**:53. DOI: 10.1038/35003523

[26] Yang X, Cai L, Liu Q. Theoretical bandgap modeling of two-dimensional triangular photonic crystals formed by interference technique of three-noncoplanar beams. Optics Express. 2003;**11**:1050-1055. DOI: 10.1364/OE.11.001050

[27] Cai L, Feng C, He M, Yang X, Meng X, Dong G, Yu X. Holographic design of a two-dimensional photonic crystal of square lattice with pincushion columns and large complete band gaps. Optics Express. 2005;**13**:4325. DOI: 10.1364/OPEX.13.004325

[28] Dong G, Cai L, Yang X, Shen X, Meng X, Xu X, Wang Y. Analysis of structure and band gap evolution of photonic crystals formed holographically by symmetric umbrella configuration

with varying apex angles. Journal of Physics D: Applied Physics. 2006;**39**:3566. DOI: 10.1088/0022-3727/39/16/007

[29] Dong G, Cai L, Yang X, Shen X, Meng X, Xu X, Wang Y. Holographic design and band gap evolution of photonic crystals formed with five-beam symmetric umbrella configuration. Optics Express. 2006;**14**:8096-8102. DOI: 10.1364/OE.14.008096

[30] Cai L, Liu Q, Yang X. Polarization optimization in the interference of four umbrellalike symmetric beams for making three-dimensional periodic microstructures. Applied Optics. 2002;**41**:6894. DOI: 10.1364/AO.41.006894

[31] Cai L, Yang X, Liu Q, Wang Y. What kind of Bravais lattices can be made by the interference of four umbrellalike beams? Optics Communications. 2003;**224**:243-246. DOI: 10.1016/j.optcom.2003.07.004

[32] Meisel D, Wegener M, Busch K. Three-dimensional photonic crystals by holographic lithography using the umbrella configuration: Symmetries and complete photonic band gaps. Physical Review B. 2004;**70**:165104. DOI: 10.1103/PhysRevB.70.165104

[33] Chan T, Toader O, John S. Photonic band gap templating using optical interference lithography. Physical Review E. 2005;**71**:046605. DOI: 10.1103/PhysRevE.71.046605

[34] Dong G, Yang X, Cai L, Shen X, Wang Y. Improvement of transmission properties through two-bend resonance by holographic design for a two-dimensional photonic crystal waveguide. Optics Express. 2008;**16**:15375. DOI: 10.1364/OE.16.015375

[35] Dong G, Yang X, Cai L. Transmission properties of an air waveguide with left-handed holographic photonic crystal cladding. 中国物理快报:英文版. 2011;**28**:014210. DOI: 10.1088/0256-307X/28/1/014210

[36] Cui X, Hafner C, Vahldieck R, Robin F. Sharp trench waveguide bends in dual mode operation with ultra-small photonic crystals for suppressing radiation. Optics Express. 2006;**14**:4351. DOI: 10.1364/OE.14.004351

[37] Smajic J, Hafner C, Erni D. Design and optimization of an achromatic photonic crystal bend. Optics Express. 2003;**11**:1378. DOI: 10.1364/OE.11.001378

[38] Chutinan A, Noda S. Waveguides and waveguide bends in two-dimensional photonic crystal slabs. Physical Review B. 2000;**62**:4488-4492. DOI: 10.1103/PhysRevB.62.4488

[39] Sakoda K. Optical Properties of Photonic Crystals. Berlin, Heidelberg: Springer; 2005. DOI: 10.1007/978-3-662-14324-7

[40] Cheng Q, Cui T. High-power generation and transmission through a left-handed material. Physical Review B. 2005;**72**:113112. DOI: 10.1103/PhysRevB.72.113112

[41] Jiang T, Zhao J, Feng Y. Stopping light by an air waveguide with anisotropic metamaterial cladding. Optics Express. 2009;**17**:170. DOI: 10.1364/OE.17.000170

[42] Dong G, Cai L, Yang X. Anomalous refractive effects in honeycomb lattice photonic crystals formed by holographic lithography. Optics Express. 2010;**18**:16302. DOI: 10.1364/OE.18.016302

[43] Dong G, Zhou J, Yang X, Meng X. Multi-refraction with same polarization state in two dimensional triangular photonic crystals. Progress in Electromagnetics Research. 2012;**128**: 91-103. DOI: 10.2528/PIER12040306

[44] Notomi M. Theory of light propagation in strongly modulated photonic crystals: Refractionlike behavior in the vicinity of the photonic band gap. Physical Review B. 2000; **62**:10696-10705. DOI: 10.1103/PhysRevB.62.10696

[45] Matsumoto T, Eom K, Baba T. Focusing of light by negative refraction in a photonic crystal slab superlens on silicon-on-insulator substrate. Optics Letters. 2006;**31**:2786-2788. DOI: 10.1364/OL.31.002786

[46] Dong G, Zhou J, Yang X, Cai L. Dual-negative refraction in photonic crystals with hexagonal lattices. Optics Express. 2011;**19**:12119-12124. DOI: 10.1364/OE.19.012119

[47] Dong G, Zhou J, Yang X, Meng X. Precise identification of Dirac-like point through a finite photonic crystal square matrix. Scientific Reports. 2016;**6**:36712. DOI: 10.1038/srep36712

[48] Dong G, Zhou J, Cai L. Zero phase delay induced by wavefront modulation in photonic crystals. Physical Review B. 2012;**87**:125107. DOI: 10.1103/PhysRevB.87.125107

[49] Yun S, Jiang Z, Xu Q, Liu Z, Werner D, Mayer T. Low-loss impedance-matched optical metamaterials with zero-phase delay. ACS Nano. 2012;**6**:4475. DOI: 10.1021/nn3012338

[50] Zhang F, Houzet G, Lheurette E, Lippens D, Chaubet M, Zhao X. Negative-zero-positive metamaterial with omega-type metal inclusions. Journal of Applied Physics. 2008;**103**:084 312. DOI: 10.1063/1.2910831

[51] Alù A, Silveirinha MG, Salandrino A, Engheta N. Epsilon-near-zero metamaterials and electromagnetic sources: Tailoring the radiation phase pattern. Physical Review B. 2007;**75**: 155410. DOI: 10.1103/PhysRevB.75.155410

[52] Mocella V, Cabrini S, Chang A, et al. Self-collimation of light over millimeter-scale distance in a quasi-zero-average-index metamaterial. Physical Review Letters. 2009;**102**:133902. DOI: 10.1103/PhysRevLett.102.133902

[53] Silveirinha M, Engheta N. Tunneling of electromagnetic energy through subwavelength channels and bends using epsilon-near-zero materials. Physical Review Letters. 2006;**97**:157403. DOI: 10.1103/PhysRevLett.97.157403

[54] Belov P, Zhao Y, Tse S, et al. Transmission of images with subwavelength resolution to distances of several wavelengths in the microwave range. Physical Review B. 2008;**77**:193 108. DOI: 10.1103/PhysRevB.77.193108

[55] Podolskiy V, Pollard R, Murphy A, et al. Optical nonlocalities and additional waves in epsilon-near-zero metamaterials. Physical Review Letters. 2009;**102**:127405. DOI: 10.1103/ PhysRevLett.102.127405

[56] Edwards B, Alù A, Young M, Silveirinha M, Engheta N. Experimental verification of epsilon-near-zero metamaterial coupling and energy squeezing using a microwave waveguide. Physical Review Letters. 2008;**100**:033903. DOI: 10.1103/PhysRevLett.100.033903

[57] Kocaman S, Aras M, Hsieh P, et al. Zero phase delay in negative-refractive-index photonic crystal superlattices. Nature Photonics. 2011;**5**:499-505. DOI: 10.1038/nphoton.2011.129

[58] Huang X, Lai Y, Hang Z, Zheng H, Chan C. Dirac cones induced by accidental degeneracy in photonic crystals and zero-refractive-index materials. Nature Materials. 2011;**10**:582. DOI: 10.1038/nmat3030

[59] D'Aguanno G, Mattiucci N, Conti C, Bloemer M. Field localization and enhancement near the Dirac point of a finite defectless photonic crystal. Physical Review B. 2013;**87**:085135. DOI: 10.1103/PhysRevB.87.085135

[60] Chan C, Hang Z, Huang X. Dirac dispersion in two-dimensional photonic crystals. Advances in OptoElectronics. 2012;**2012**:313984. DOI: 10.1155/2012/313984

[61] Zandbergen S, de Dood M. Experimental observation of strong edge effects on the pseudodiffusive transport of light in photonic graphene. Physical Review Letters. 2010;**104**:043903. DOI: 10.1103/PhysRevLett.104.043903

IntechOpen